Talanta 80 (2010) 2016–2022

Contents lists available at ScienceDirect

Talanta

journal homepage: www.elsevier.com/locate/talanta

SiO_2 coated Fe_3O_4 magnetic nanoparticle dispersed multiwalled carbon nanotubes based amperometric glucose biosensor

Tessy Theres Baby, S. Ramaprabhu*

Alternative Energy and Nanotechnology Laboratory (AENL), Nano Functional Materials Technology Centre (NFMTC), Department of Physics, Indian Institute of Technology Madras, Chennai, India

ARTICLE INFO

Article history:
Received 22 August 2009
Received in revised form 31 October 2009
Accepted 2 November 2009
Available online 10 November 2009

Keywords:
Amperometric
Vibrating sample magnetometer
Bioelectrode
CNTs
Biosensor

ABSTRACT

A new type of amperometric glucose biosensor based on silicon dioxide coated magnetic nanoparticle decorated multiwalled carbon nanotubes (Fe_3O_4@SiO_2/MWNTs) on a glassy carbon electrode (GCE) has been developed. MWNTs have been synthesized by catalytic chemical vapour decomposition (CCVD) of acetylene over rare earth (RE) based AB_3 alloy hydride catalyst. The as-grown MWNTs have been purified and further functionlized. Functionalized MWNTs have been decorated with magnetic Fe_3O_4 nanoparticles which have been uniformly coated with biocompatible SiO_2 using a simple chemical reduction method. The characterization of magnetic nanoparticle modified MWNTs have been done by X-ray diffraction (XRD), Fourier transform infra red spectroscopy (FT-IR), scanning electron microscope (SEM), transmission electron microscope (TEM), vibrating sample magnetometer (VSM), energy dispersive X-ray analysis (EDX) and UV–vis spectroscopy. Amperometric biosensor has been fabricated by the deposition of glucose oxidase (GOD) over Nafion-solubilized Fe_3O_4@SiO_2/MWNTs electrode. The resultant bioelectrode retains its biocatalytic activity and offers fast and sensitive glucose quantification. The performance of the biosensor has been studied using cyclic voltammetry and amperometry and the results have been discussed. The fabricated glucose biosensor exhibits a linear response from 1 μM to 30 mM with an excellent detection limit of 800 nM indicating the potential applications in food industries.

1. Introduction

Magnetic core–shell Fe_3O_4@SiO_2 nanoparticles as specially immobilizing carrier of biomolecules have aroused great interest in current researches. The inner iron oxide core with outer shell of silica not only stabilizes the nanoparticles in solution but also provides sites for surface modification with various biomedical ligands in biomedical applications. The coating of silica on the magnetic nanoparticles facilitated the dispersion of nanoparticles [1,2]. Due to their unique physical, chemical, and mechanical properties, superparamagnetic composite nanoparticles (NPs) hold much promise for biosensor applications [3–5]. Superparamagnetic iron oxide core of individual NPs becomes more efficient at dephasing the spins of surrounding water protons, enhancing spin–spin relaxation times (T_2 relaxation times) so that the NPs act as magnetic relaxation switches (MRS) [6]. Carbon nanotubes (CNTs) are one of the most studied nanomaterials for application in biosensor technologies, by immobilizing bioactive molecules on their surfaces through covalent or non-covalent bonds. The nanodimensions of CNTs guarantee a very large active surface area and are especially suited for the conception of miniaturized sensors. In addition to this, high porosity and reactivity makes them ideal candidates for the storage of neutral species as well as electron donors when used as electrodes in electrochemical reactions [7–9].

Compared with the corresponding CNTs-free biosensor, the CNTs-doped counterpart exhibited enhanced stability and sensitivity. Surface functionalization aids CNTs to become biocompatible, improving their solubility in physiological solutions and selective binding to biotargets. CNTs functionalization with biomolecules may occur by adsorption, but covalent tethering provides better stability, accessibility, selectivity and reduced leaching, and usually occurs by an amidation reaction [10]. CNTs are also used for dramatically amplifying enzyme-based bioaffinity electrical sensing of proteins and DNA [11]. Compared with single walled nanotubes (SWNTs), much cheaper multiwalled nanotubes (MWNTs) produced by chemical vapour deposition have more structural defects and thus provide more sites for biomolecule immobilization [8]. Non-covalently functionalized CNTs may also immobilize glucose and small molecules [12].

Nanocomposite materials may play an important role for improving functionalized electrodes envisaging commercial applications. Nanoparticles, especially metal nanoparticles, are an emerging issue in biosensor design, and they have been combined with CNTs to modify a glassy carbon electrode, thus improving the

* Corresponding author. Tel.: +91 44 22574862; fax: +91 44 22570509.
E-mail address: ramp@iitm.ac.in (S. Ramaprabhu).

0039-9140/$ – see front matter © 2009 Elsevier B.V. All rights reserved.
doi:10.1016/j.talanta.2009.11.010

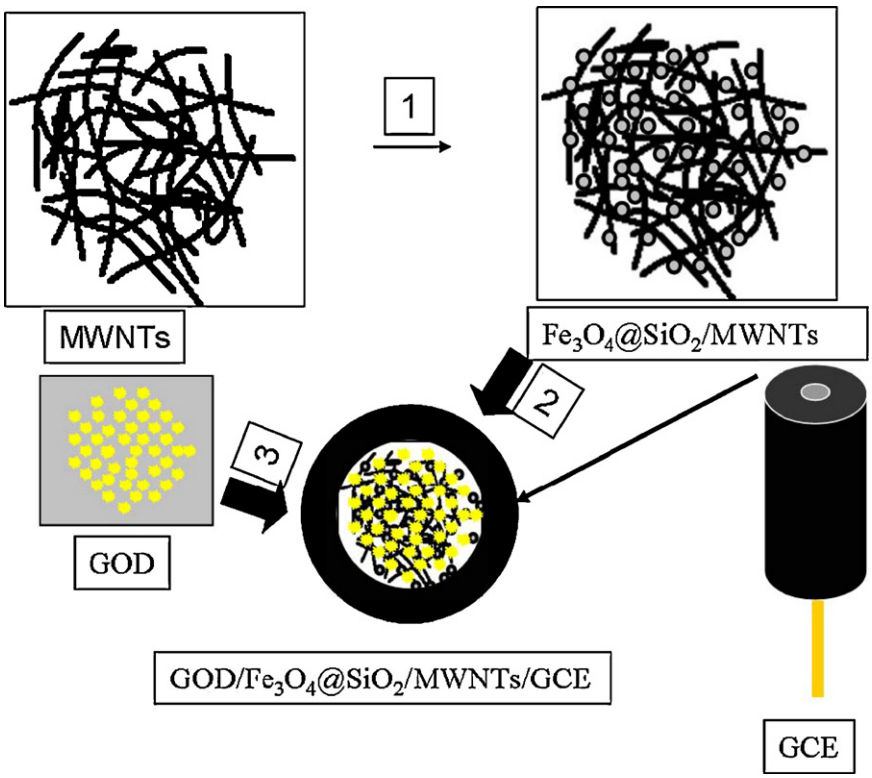

Fig. 1. Schematic of fabricated GOD/Fe_3O_4@SiO_2/MWNTs/GC electrode.

electroactivity and selectivity for glucose [13]. Metal nanoparticles have been applied as catalysts in numerous biosensor applications, due to their superior stability and complete recovery in biochemical redox processes. However, other groups showed that immobilization of the Au nanoparticles (or other metal nanoparticles) on the electrode surface would also cause similar catalytic effect on the electrochemical responses. Amperometric detection of glucose was developed using Au nanoparticles and CNT-multilayer membranes [14].

An electrochemical study with cyclic voltammetry and impedance analysis confirmed that glucose oxidase molecules suffer minimal structure changes after being immobilized on the surface of CNTs, retaining the ability to interact with small biomolecules (e.g., ethidium bromide) [7]. In this present study, MWNTs functionalized with nitric acid, in order to introduce carboxylic acid groups, have been used for the preparation of Fe_3O_4@SiO_2/MWNTs-based electrodes. Prior to immobilization, glucose oxidase (GOD) was physically adsorbed on these modified electrodes. Here, we show a good performance, fast response, nice stability and reproducibility, and a low detection limit of Fe_3O_4@SiO_2/MWNTs nanocomposite based on the reduction of H_2O_2 by immobilizing glucose oxidase on the composite.

2. Experimental

2.1. Materials

Glucose oxidase (GOD, from *Aspergillus niger*), tetraethoxysilane (TEOS) were purchased from Sigma. 0.1 M phosphate buffer solution (PBS, pH 7) prepared using potassium phosphate dibasic anhydrous and potassium dihydrogen orthophosphate. Ferric chloride ($FeCl_3{\cdot}6H_2O$), ferrous sulphate ($FeSO_4{\cdot}7H_2O$), ethanol and ammonium hydroxide (25%) were of analytical grade and deionised (dI) water was used throughout.

2.2. Sample preparation

Carbon nanotubes were synthesized by catalytic chemical vapour deposition over an alloy hydride catalyst. Rare earth based AB_3 alloy hydride was made by arc melting followed by several cycle of hydrogen absorption/desorption process. The catalyst was kept inside a furnace and acetylene (carbon precursor) was allowed at a temperature range 650–750 °C, in an inert atmosphere. Pyrolysis of acetylene was taken place at that temperature and MWNTs start growing. The as-grown MWNTs were purified before using for any applications. The amorphous carbon can be removed by heating the as-grown sample in oxygen atmosphere. Refluxing in concentric acids has been shown to be an

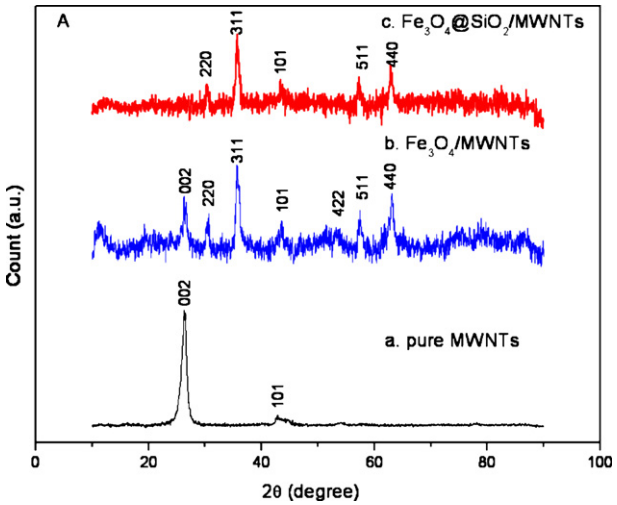

Fig. 2. X-ray diffractograms of (a) pure MWNTs, (b) Fe_3O_4/MWNTs and (c) Fe_3O_4@SiO_2/MWNTs.

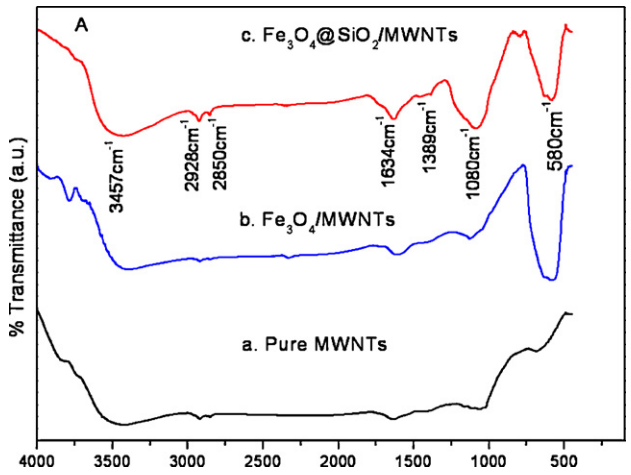

Fig. 3. FT-IR spectrum of (a) pure MWNTs, (b) Fe_3O_4/MWNTs and (c) Fe_3O_4@SiO_2/MWNTs.

effective method for the separation of the catalytic impurities [15].

Hydrated ferric chloride and ferrous sulphate precursors were dissolved in 100 ml water and heated to 90 °C, and then two solutions, 10 ml of ammonium hydroxide (25%) and 0.5 g of functionalized MWNTs dissolved in 50 ml of water, were added rapidly and sequentially. The mixture was stirred at 90 °C for 30 min and then cooled to room temperature. The black precipitate was collected by filtrating and washed to neutral with water. The obtained black precipitate was Fe_3O_4/MWNT nanoparticles and was ready for use.

Core–shell Fe_3O_4@SiO_2/MWNT nanoparticles were prepared by growing silica layers onto the surface of the Fe_3O_4/MWNTs as described by Lu et al. [16]. Twenty-five milliliters of ethanol, 1 ml water, 1 ml ammonium hydroxide and 150 μl of TEOS were added in a 250 ml three neck flask in a 40 °C water bath. Add Fe_3O_4/MWNTs to the above solution under mechanical stirring. Aliquots of the mixture were takes out after 12 h by centrifugation and washed with dI water and vacuum-dried at 50 °C overnight.

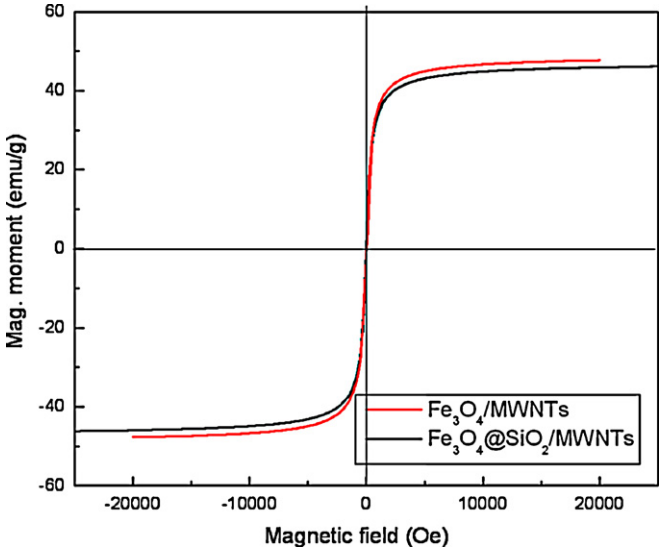

Fig. 4. VSM study of Fe_3O_4/MWNTs (red line) and Fe_3O_4@SiO_2/MWNTs (black line). (For interpretation of the references to color in this figure legend, the reader is referred to the web version of the article.)

2.3. Fabrication of the amperometric immunosensor

The GCE (3-mm diameter) was first polished on chamois leather with 0.05-μm alumina slurry and then washed ultrasonically in doubly distilled water, anhydrous ethanol, and doubly distilled water, respectively. The cleaned GCE was allowed to dry at room temperature.

Fe_3O_4@SiO_2/MWNTs was sonicated in 0.5% Nafion solution to give a concentration of ~1 mg/ml. For example, four microliters of the Fe_3O_4@SiO_2/MWNTs suspension was film-cast onto the surface of the GC electrode and allowed to dry slowly. Films formed from Nafion-solubilized MWNTs are more uniform and stable than those cast from organic solvents. Nafion assists the dispersion of Fe_3O_4@SiO_2/MWNTs, whereby the Fe_3O_4@SiO_2/MWNTs remains well dispersed on prolonged standing. 16 μl of 100 U GOD solution was film-cast onto the surface of the Fe_3O_4@SiO_2/MWNTs/GC electrode and allowed to dry slowly at 4 °C. The obtained Fe_3O_4@SiO_2/MWNTs/GC electrode was washed carefully with DI water and dried at less than 4 °C. Fig. 1 shows the schematic of fabrication of Fe_3O_4@SiO_2/MWNTs/GC electrode. These Fe_3O_4@SiO_2/MWNTs/GC electrodes were coated with an extra 2.5 μl layer of 0.5% Nafion. The electrodes were rinsed with pH 7 phosphate buffer solution (PBS) and stored in the buffer at 4 °C prior to use.

2.4. Characterization methods

The electrochemical measurements were performed with CH Instruments CHI 608C Electrochemical Analyzer/Workstation. A platinum wire counter electrode, Ag/AgCl (3 M KCl) reference electrode and glassy carbon electrode (GCE, diameter 3 mm) were inserted into a modified 5–10 ml glass cell for the measurement. All potentials are referred to the Ag/AgCl reference electrode. The samples were characterized using different techniques. Powder X-ray diffraction studies were carried out using a X'Pert PRO, PANalytical diffractometer with nickel-filtered Cu Kα radiation as the X-ray source. The sample was scanned in steps of 0.016° in the 2θ range 10–90°. Identification and characterization of functional groups were carried out using PerkinElmer FT-IR spectrometer in the range 300–4000 cm^{-1}. The surface morphology of the sample was done by using scanning tunneling microscope (SEM) (FEI; QUANTA scanning electron microscope) with EDX system. The EDX system attached with the SEM enables the elemental analysis of the samples. The TEM images were obtained on a transmission electron microscope (TEM, JEOL JEM-2010F). UV absorption spectra of the samples in deionized water were recorded on JASCO Corp., V-570 spectrophotometer. Magnetic study of the samples had been done by vibrating sample magnetometer (VSM).

3. Results and discussion

3.1. XRD and FT-IR studies of the samples

The XRD pattern in Fig. 2 indicates that the crystal structure of magnetic nanocomposites comprises MWNTs, two phases of cubic Fe_3O_4/MWNTs and Fe_3O_4@SiO_2/MWNTs. Well-resolved diffraction peaks reveal the good crystallinity of the Fe_3O_4 specimens, which are located at 2θ of 30.28°, 35.56°, 43.3°, 53.68°, 57.36° and 62.72°, respectively. These data matched well with the peer Ref. [17]. The peaks in the Fe_3O_4@SiO_2/MWNTs reveal that even after the SiO_2 coating the sample retains its crystallinity [18]. The absence of SiO_2 peak in the XRD pattern in the composite is due to its amorphous structure coated on the Fe_3O_4 nanoparticles. The diffraction peak at 2θ = 26.4° is the typical Bragg peak of pristine MWNTs and can be indexed to the (0 0 2) reflection of graphite. Judging from the pat-

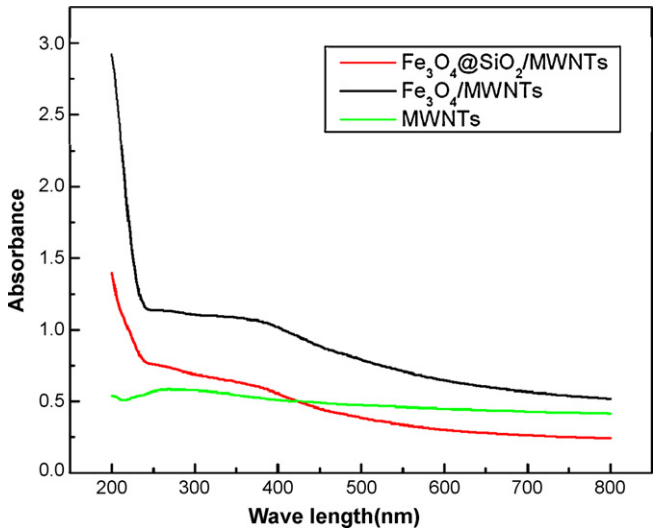

Fig. 5. UV–vis absorbance study of pure MWNTs (green), Fe_3O_4/MWNTs (black) and Fe_3O_4@SiO_2/MWNTs (red). (For interpretation of the references to color in this figure legend, the reader is referred to the web version of the article.)

tern, the third phase does not exist. The average grain size (D) of the Fe_3O_4 particles was calculated using Scherrer's formula described by

$$D = \frac{0.9\lambda}{\beta \cos(\theta)} \quad (1)$$

λ is wave length of X-ray used, β is FWHM of diffraction peak and θ angle corresponding to the peak. The calculated average grain sizes using 35.56° diffraction peak were ~25 nm. Moreover, the diffractive peaks of Fe_3O_4 are broadened, implying that the crystalline size of Fe_3O_4 particles is quite small.

Selectivity of MWNTs-based biosensors may be introduced by anchoring on the MWNTs surface, specific functional groups that selectively bind specific target molecules. All types of MWNTs show peaks between 1300 and 1100 cm^{-1}, which are ascribed to the phenyl-carbonyl C–C stretch bonds (Fig. 3(a)). The peak between 3300–3500 cm^{-1} is normally due to stretching vibration mode of OH and NH group. The peak at 3457 cm^{-1} in curve (a) and curve (b) is due to OH group (due to oxidation with HNO_3) and in curve (c) it is due to both OH and –NH (from ammonia solution). One can see a small broadening of this peak in the case of curve (c). As seen from Fig. 3(b), the peak at 568 cm^{-1} is the stretching vibration due to the interactions of Fe–O–Fe in Fe_3O_4 and the peaks at 1383, 2850 and 2928 cm^{-1} are attributed to the in-plane bending vibration of methyl ($-CH_3$) and the symmetric and asymmetric vibration of methylene ($-CH_2-$). Compared with the two spectra (b and c), the existence of the characteristic Si–O–Si peak at 1080 cm^{-1} in Fig. 3(c) is direct evidence to verify the formation of the silica shell. From Fig. 3(b) and (c), we can also see that the characteristic Fe–O–Fe peak of Fe_3O_4/MWNTs at 568 cm^{-1} shift to 580 cm^{-1} in the spectrum of SiO_2 coated magnetic nanoparticles. It is inferred that the silica shell is linked to the surface of the magnetic nanoparticles by a Fe–O–Si chemical bond [19]. It is generally accepted that the interpretation of surface groups can only be qualitative, as they cannot be expected to behave as isolated functional groups [20].

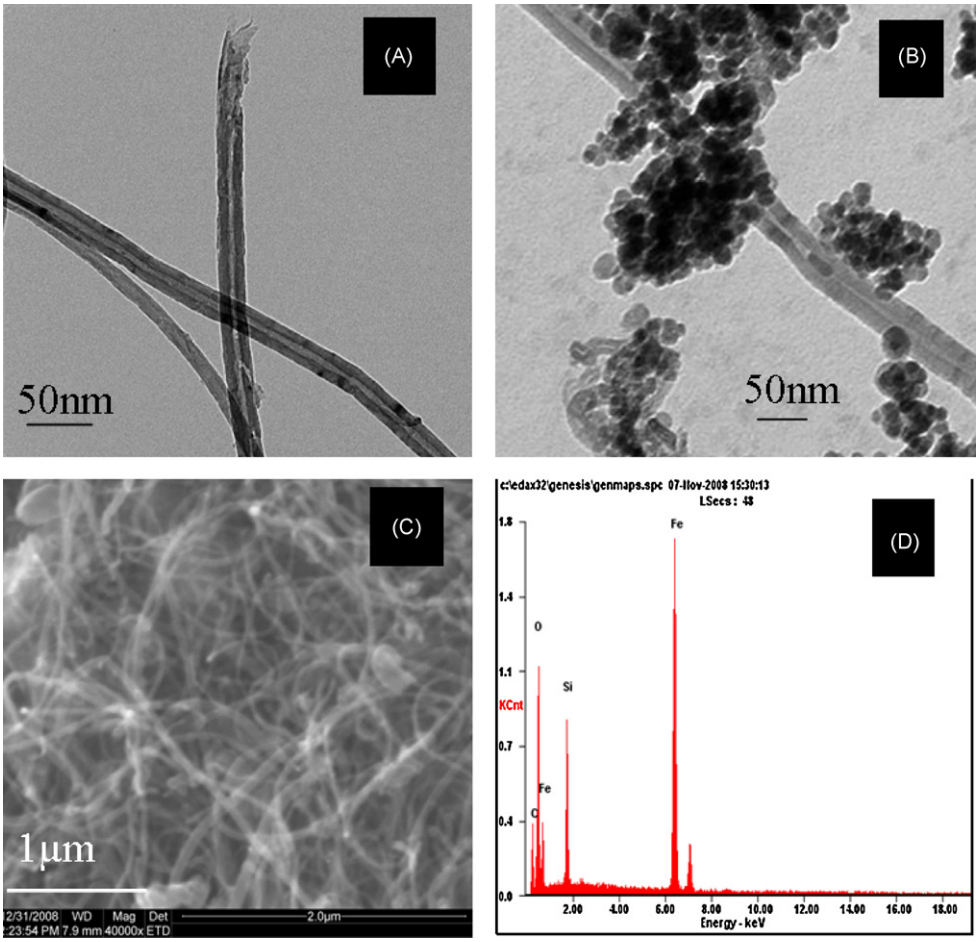

Fig. 6. TEM image of (A) pure MWNTs, (B) Fe_3O_4@SiO_2/MWNTs, (C) SEM image of pure MWNTs and (D) EDX for Fe_3O_4@SiO_2/MWNTs.

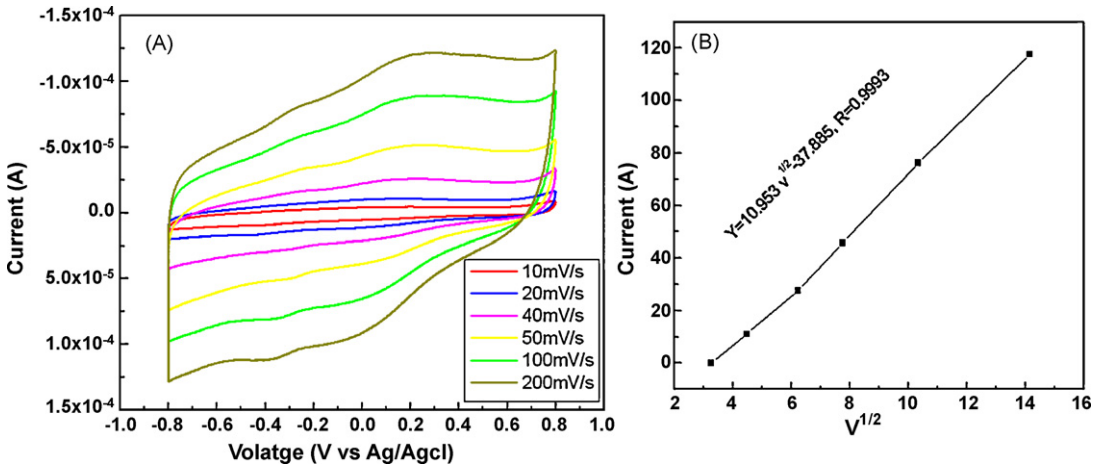

Fig. 7. (A) Fe_3O_4@SiO_2/MWNTs modified electrode at different scan rates in PBS (0.1 M, pH 7) and (B) the plot of peak anodic peak current vs. $v^{1/2}$.

3.2. Magnetic and optical studies of samples

Fig. 4 exhibits the hysteresis loop of the as-prepared sample at room temperature. It can be seen that the saturation magnetization of Fe_3O_4@SiO_2/MWNTs (~44 emu/g) is almost comparable to that of Fe_3O_4/MWNTs (~46 emu/g), which indicates that Fe_3O_4 nanoparticles covered by a silica network can preserve their superparamagnetic properties.

The UV–vis absorption spectrum of different samples in deionized water is illustrated in Fig. 5. A very broad absorption peak appeared at about 267 nm, which originated from the C=C structure of MWNTs [21]. The optical properties of all the magnetic nanoparticles used (with or without silica coating) are dominated by a broad featureless absorption tail characteristic of indirect band gap semiconductors. In the wavelength of >330 nm region, a broad featureless adsorption could be observed in the curves with SiO_2 and without SiO_2 originates primarily from the absorption and scattering of light by magnetic particles, which is in accordance with the previous literatures [22], and is the characteristic of indirect band gap semiconductors [23].

3.3. SEM and TEM analysis of the samples

The morphology of the purified MWNTs is clearly visible from the SEM image shown in Fig. 6(C). Fig. 6(A and B) illustrates the TEM images of the synthesized MWNTs and prepared Fe_3O_4@SiO_2/MWNTs core–shell nanoparticles. The open end of the MWNTs are clearly visible from the TEM image. The diameter of the MWNTs is ~25 nm. With the help of references [24,25] and the TEM and EDX shown in Fig. 6(B and D) we can see that the sample is nearly in core–shell structures, with black color shows Fe_3O_4 and ash color is the SiO_2 shell. This indicates the successful coating on the surface of the magnetic particles with silica. The EDX shown in Fig. 6(D) confirms the presence of iron and silicon in the sample. Inorganic compound functionalized iron oxide NPs can greatly enhance the antioxidation properties for naked iron oxide NPs, and its corresponding scope of application has been greatly extended. Moreover, inorganic compounds functionalized iron oxide NPs are very promising for application in catalysis, biolabeling, and bioseparation [26].

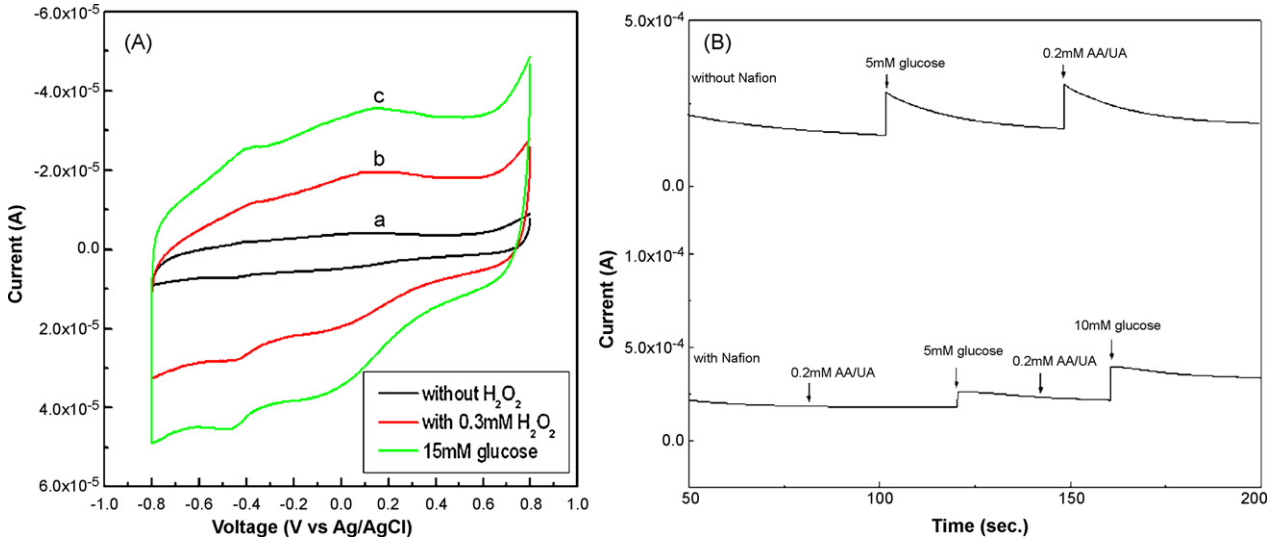

Fig. 8. (A) displays the CV of the Fe_3O_4@SiO_2/MWNTs modified electrode (a) in PBS (b) with 0.3 mM H_2O_2 and (c) 15 mM glucose solution and (B) study of interference due to ascorbic acid and uric acid with and without a selective Nafion film on the GOD/Fe_3O_4 @SiO_2/MWNTs modified electrode.

3.4. Cyclic voltammetry and electrocatalytic properties of the GOD/Fe_3O_4@SiO_2/MWNTs modified electrode toward hydrogen peroxide

Cyclic voltammetry peak currents of the GOD/Fe_3O_4@SiO_2/MWNTs modified electrode increased with scan rate and the peak separation (ΔE_p) was nearly independent of the scan rate (Fig. 7(A)). The anodic peak currents increased linearly with the increase of the square root of scan rate, suggesting that the electrochemical reaction is a diffusion-controlled process (Fig. 7(B)).

Fig. 8(A) shows the cyclic voltammograms of the GOD/Fe_3O_4@SiO_2/MWNTs/GC electrode in the absence (curve a), in the presence of 0.3 mM H_2O_2 (curve b) and in 15 mM glucose solution (curve c). The GOD/Fe_3O_4@SiO_2/MWNTs/GC electrode exhibits significant electrocatalysis to the oxidation and reduction of H_2O_2 starting around 0.1 V, which is even lower than that obtained with the GOD/MWNTs electrode by covalent binding immobilization (0.2 V) [27]. The good performance of the fabricated GOD/Fe_3O_4@SiO_2/MWNTs/GC electrode toward the oxidation of H_2O_2 makes it attractive for glucose sensing applications. When MWNTs were treated with the acid solution, the carboxylic acid functional groups introduced at the end points and surface of MWNTs allow them to adsorb the enzyme of GOD. Since this adsorption was fulfilled through a covalent bond, the link between MWNTs and GOD was more close and stable. Moreover, because the MWNTs have large surface area, they could enhance a large amount of GOD to be immobilized within the nanotubes. The more quantity of GOD made the biosensor possible to engender high response current and expand the detectable range when in a glucose solution.

3.5. Effect of electroactive interferents

The interference of some electroactive compounds to the glucose response was examined. To study this we added 0.2 mM of ascorbic acid (AA) and uric acid (UA) to the solution and checked the GOD/Fe_3O_4@SiO_2/MWNTs/GC electrode with Nafion coating and without Nafion coating. The upper curve in Fig. 8(B) which had been done without Nafion shows the presence of AA and UA. The lower curve in Fig. 8(A) shows the interference study with Nafion coated GOD/Fe_3O_4@SiO_2/MWNTs/GC electrode. There is not much change in the current due to AA and UA. Which clearly shows that 2.5 μl of 0.5 wt% Nafion on the surface of GOD/Fe_3O_4@SiO_2/MWNTs/GC electrode prevent the interference.

3.6. Study of amperometric i–t and calibration curve

The amperometric responses at the GOD/Fe_3O_4@SiO_2/MWNTs/GC electrode for successive addition of different concentration of glucose are presented in Fig. 9 (inset). Well-defined current responses for glucose were obtained at the GOD/Fe_3O_4@SiO_2/MWNTs/GC electrode. The reaction occurring at the biosensor is very fast in reaching a dynamic equilibrium upon each addition of the sample solution, generating a steady-state current signal within 3–6 s. Using the optimum conditions established in the above studies, the calibration of the GOD/Fe_3O_4@SiO_2/MWNTs/GC electrode is depicted in Fig. 9. The steady-state currents gradually increased with increasing concentration of glucose, and exhibited a linear relationship with the concentration of glucose in the range from 1 μM to 30 mM with a detection limit of 800 nM (estimated at S/N = 3) with a correlation coefficient of 0.9994. The performance of GOD/Fe_3O_4@SiO_2/MWNTs/GC electrode is superior than the reported value of GOD/Fe_3O_4@SiO_2/GC electrode which is having

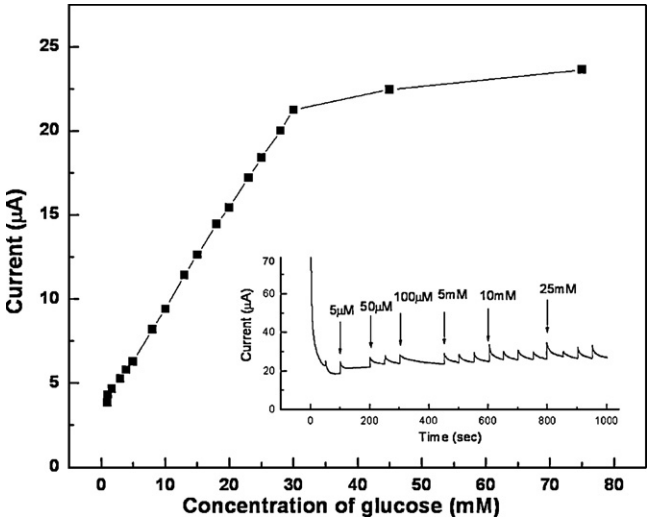

Fig. 9. The calibration curve of the fabricated GOD/Fe_3O_4@SiO_2/MWNTs/GC electrode. Amperometric *i–t* curve with addition of different concentration of glucose solution (inset).

a linear range 1.0×10^{-5} to 4.0×10^{-3} M with a detection limit of 3.2 μM [28].

From Fig. 9, it was observed that the biosensor response gradually deviates from the linear feature as the glucose concentration up to 30 mM. This is the characteristic of a typical Michaelis–Menten kinetics. The apparent Michaelis–Menten constant $K^{app}m$, which depicts the enzyme–substrate kinetics of biosensor, can be calculated from the Line weaver–Burk equation:

$$\frac{1}{I_{ss}} = \left(\frac{K^{app}m}{I_{max}}\right)\left(\frac{1}{C}\right) + \frac{1}{I_{max}} \quad (2)$$

where C is the concentration of substrate, I_{ss} is the steady-state current and I_{max} is the maximum current measured under substrate saturation [29]. Therefore the values of the $K^{app}m$ and I_{max} in this work can be calculated to be 13 mM and 25 μA, respectively. The lower $K^{app}m$ means the higher enzymatic activity of immobilized GOD thus the above result further indicates that the Fe_3O_4@SiO_2/MWNTs modified biosensor possesses a high affinity to glucose [30].

Since MWNTs have excellent electrical conductivity, MWNTs as well as iron oxide dispersed MWNTs attached to the protein shell of enzyme could improve the transfer of electrons between the active redox center of the enzyme. This effect could accelerate the regeneration of GOD and increase the relative activity of the enzyme finally. It is thought to be the mean reason of why the current response of MWNTs and iron oxide dispersed MWNTs modified glucose biosensor was higher than that of the other biosensors.

4. Conclusion

Fe_3O_4 nanoparticles can be successfully stabilized by SiO_2 and Fe_3O_4@SiO_2/MWNTs can be deposited on GCE. GOD can be effectively immobilized on Fe_3O_4@SiO_2/MWNTs/GC electrode to produce a fast direct electron transfer. The immobilized GOD maintains its bioactivity and native structure. Its reduced form can be oxidized by dissolved oxygen to cause an electrocatalytic reaction, which is restrained by glucose due to the reaction between the oxidized form of GOD and glucose. Based on the decrease of electrocatalytic response, a novel glucose sensor has been developed and the resulting sensor displays a high sensitivity (58.9 μA/mM cm^2) and a linear range from 1 μM to 30 mM for glucose determination, and can efficiently exclude the interference of commonly coexisted uric and ascorbic acid. Because of its convenient preparation and

good properties, this biosensor can be used for glucose determination in food industries.

Acknowledgements

The authors acknowledge the funding AOARD, USA and Indian Institute of Technology Madras (IITM).

References

[1] K.H. See, M.E. Mullins, O.P. Mills, P.A. Heiden, Nanotechnology 16 (2005) 1950–1959.
[2] Z.M. Liu, Y.L. Liu, H.F. Yang, Y. Yang, G.L. Shen, R.Q. Yu, Anal. Chim. Acta 533 (2005) 3–9.
[3] J. Heitmann, F. Muller, M. Zacharias, U. Gosele, Adv. Mater. 17 (2005) 795–803.
[4] A.D. Wellman, M.J. Sepaniak, Anal. Chem. 78 (2006) 4450–4456.
[5] X.Y. Zhao, S.A. Shippy, Anal. Chem. 76 (2004) 1871–1876.
[6] L. Josephson, J.M. Perez, R. Weissleder, Angew. Chem. Int. Ed. 40 (2001) 3204–3206.
[7] S. Daniel, T.P. Rao, K.S. Rao, S.U. Rani, G.R.K. Naidu, H.-Y. Lee, T. Kawai, Sens. Actuators B 122 (2007) 672–682.
[8] M. Guo, J. Chen, D. Liu, L. Nie, S. Yao, Bioelectrochemistry 62 (2004) 29–35.
[9] H.Z. Geng, X.B. Zhang, S.H. Mao, A. Kleinhammes, H. Shimoda, Y. Wu, O. Zhou, Chem. Phys. Lett. 399 (2004) 109–113.
[10] K. Jiang, L.S. Schadler, R.W. Siegel, X. Zhang, H. Zhang, M. Terrones, J. Mater. Chem. 14 (2004) 37–39.
[11] Z.M. Tahir, E.C. Alocilja, D.L. Grooms, Biosens. Bioelectron. 20 (2005) 1690–1695.
[12] R.J. Chen, D. Zhang, H.D. Wang, J. Am. Chem. Soc. 123 (2001) 3838–3839.
[13] K.B. Male, S. Harpovic, Y. Liu, D. Wang, J.H.T. Luong, Anal. Chim. Acta 516 (2004) 35–41.
[14] Y. Liu, S. Wu, H. Ju, L. Xu, Electroanalysis (NY) 19 (2007) 986–989.
[15] I.W. Chiang, B.E. Brinson, R.E. Smalley, J.L. Margrave, R.H. Hauge, J. Phys. Chem. B 157 (2001) 1105–1161.
[16] Z. Lu, J. Dai, X. Song, G. Wang, W. Yang, Colloids Surf. A 317 (2008) 450–456.
[17] Q. Lan, C. Liu, F. Yang, S.Y. Liu, J. Xu, D.J. Sun, J. Colloid Interface Sci. 310 (2007) 260–269.
[18] S.L. Tie, C.H. Lee, Y.S. Bae, M.B. Kim, K. Lee, C.H. Lee, Colloid Surf. A 293 (2007) 278–285.
[19] F.H. Chen, Q. Gao, J.Z. Ni, Nanotechnology 19 (2008) 165103.
[20] M.S.P. Shaffer, X. Fan, A.H. Windle, Carbon 36 (1998) 1603–1612.
[21] C.S. Chen, X.H. Chen, B. Yi, T.G. Liu, W.H. Li, L.S. Xu, Z. Yang, H. Zhang, Y.G. Wang, Acta Mater. 54 (2006) 5401–5407.
[22] M.A. Correa-Duarte, M. Giersig, N.A. Kotov, L.M. Liz-Marzán, Langmuir 14 (1998) 6430–6435.
[23] G. Dagan, W.M. Shen, M. Tomkiewicz, J. Electrochem. Soc. 139 (1992) 1855–1861.
[24] G.H. Du, Z.L. Liu, X. Xia, Q. Chu, S.M. Zhang, J. Sol–Gel Sci. Technol. 39 (2006) 285–291.
[25] Z.Z. Xu, C.C. Wang, W.L. Yang, S.K. Fu, J. Mater. Sci. 22 (2005) 4667–4669.
[26] W. Wu, H. Quanguo, C. Jiang, Nanoscale Res. Lett. 3 (2008) 97–415.
[27] C.E. Banks, R.G. Compton, Analyst 130 (2005) 1232–1239.
[28] J. Qiu, H. Peng, R. Liang, Electrochem. Commun. 9 (2007) 2734–2738.
[29] S. Zhang, W. Nü, H. Yu, Y. Niu, C. Sun, Bioelectrochemistry 67 (2005) 15–22.
[30] X. Chu, D. Duan, G. Shen, R. Yu, Talanta 71 (2007) 2040–2047.